Nanoelectronics and Its New Materials – A NEW ERA OF NANOSCIENCE

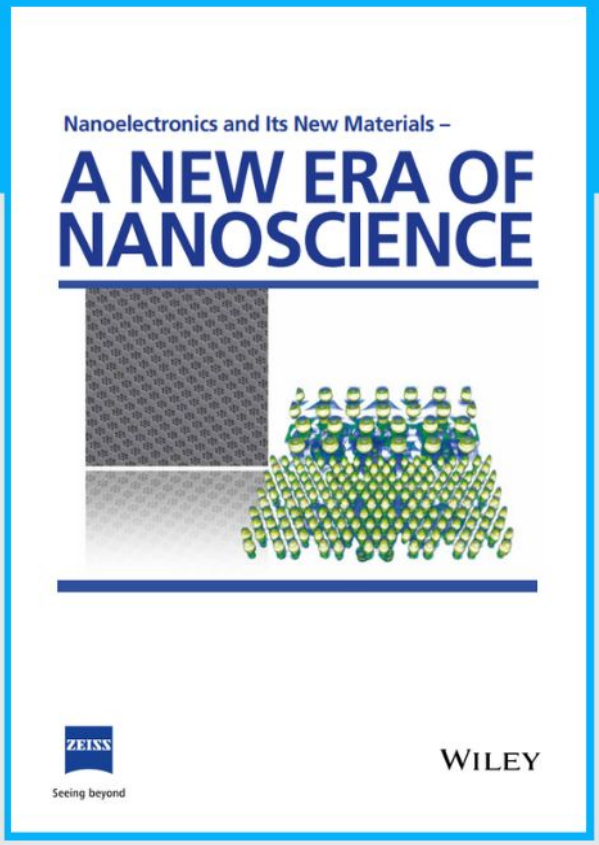

Discover the recent advances in electronics research and fundamental nanoscience.

Nanotechnology has become the driving force behind breakthroughs in engineering, materials science, physics, chemistry, and biological sciences. In this compendium, we delve into a wide range of novel applications that highlight recent advances in electronics research and fundamental nanoscience. From surface analysis and defect detection to tailored optical functionality and transparent nanowire electrodes, this eBook covers key topics that will revolutionize the future of electronics.

To get your hands on this valuable resource and unleash the power of nanotechnology, simply download the eBook now. Stay ahead of the curve and embrace the future of electronics with nanoscience as your guide.

ZEISS

Seeing beyond

WILEY

Defect-Laden $MoSe_2$ Quantum Dots Made by Turbulent Shear Mixing as Enhanced Electrocatalysts

Chongyang Zhu, Yuan Huang, Feng Xu, Peng Gao, Binghui Ge, Jing Chen, Haibo Zeng, Eli Sutter, Peter Sutter,* and Litao Sun**

***A** high density of edge sites and other defects can significantly improve the catalytic activity of layered 2D materials. Herein, this study demonstrates a novel top-down strategy to maximize catalytic edge sites of $MoSe_2$ by breaking up bulk $MoSe_2$ into quantum dots (QDs) via "turbulent shear mixing" (TSM). The ultrasmall size of the $MoSe_2$ QDs provides a high fraction of atoms in reactive edge sites, thus significantly improving the catalytic activities. The violent TSM further introduces abundant defects as additional active sites for electrocatalytic reactions. These edge-proliferated and defect-laden $MoSe_2$ QDs are found to be efficient electrocatalysts for the hydrogen evolution reaction, and useful as counter electrodes in dye-sensitized solar cells. The work provides a new paradigm for creating edge-proliferated and defect-rich QDs from bulk layered materials.*

Layered two-dimensional (LTD) materials have been studied intensely.[1] Typical LTD materials consist of 2D molecular layers held together by van der Waals forces. Exfoliation of the bulk LTD materials can afford individual layers with useful electronic, optical, and catalytic properties, among others.[2] Particularly, individual layers of transition-metal dichalcogenides (TMDs) have shown potential in photocatalysis, electrocatalysis, and energy conversion systems,[3] making them promising candidates for replacing platinum-based catalysts.[4] It has been reported that the edges of the crystal layers are favorable catalytic reaction sites of TMDs.[5] Increasing the density of edge sites can thus enhance the overall reactive activity.[6] How then to maximize edge sites? We address this question for molybdenum diselenide ($MoSe_2$) through the use of "turbulent shear mixing".

$MoSe_2$, a representative member of the TMDs family, was recently reported to have a higher intrinsic electrical conductivity and lower Gibbs free energy for hydrogen adsorption at the edges when compared to the more extensively studied MoS_2.[7] Thus, effort has been devoted to obtaining $MoSe_2$

Dr. C. Y. Zhu, Prof. F. Xu, Prof. L. T. Sun
SEU-FEI Nano-Pico Center
Key Laboratory of MEMS of the Ministry of Education
Southeast University
Nanjing 210096, China
E-mail: fxu@seu.edu.cn; slt@seu.edu.cn

Dr. Y. Huang
Center for Functional Nanomaterials
Brookhaven National Laboratory
Upton, NY 11973, USA

Prof. P. Gao
Electron Microscopy Laboratory
School of Physics
Peking University
Beijing 100871, China

Prof. B. H. Ge
Institute of Physics
Chinese Academy of Sciences
Beijing 100190, China

Dr. J. Chen
School of Electronic Science & Engineering
Southeast University
Nanjing 210096, China

Prof. H. B. Zeng
College of Materials Science and Engineering
Nanjing University of Science and Technology
Nanjing 210094, China

Prof. E. Sutter, Prof. P. Sutter
Department of Mechanical & Materials Engineering
Department of Electrical & Computer Engineering
University of Nebraska–Lincoln
Lincoln, NE 68588, USA
E-mail: psutter@unl.edu

DOI: 10.1002/smll.201700565

ADVANCED SCIENCE NEWS
www.advancedsciencenews.com

electrocatalysts with a high density of active edge sites. For example, Cui and co-workers have prepared $MoSe_2$ thin films composed of vertically aligned layers with enhanced electrocatalytic activity for the hydrogen evolution reaction (HER) that was attributed to exposed active edges.[8] Moreover, porous and defect-rich $MoSe_2$ nanosheets could provide more abundant reactive sites.[9] Composite structures such as $MoSe_2$/reduced graphene oxide (rGO), $MoSe_2$/carbon nanofibers, and $MoSe_2$/carbon nanotubes,[10–12] have further been studied with the goal of enhancing electrocatalytic activity. The catalytic properties of $MoSe_2$ quantum dots (QDs), however, have not been reported so far. Previous works on TMDs have suggested that compared to nanosheets, the QDs have larger surface areas and more edge atoms that could greatly increase their electrocatalytic activity.[13]

Herein, we have developed a new method that we refer to as "turbulent shear mixing" (TSM) to efficiently break up bulk $MoSe_2$ crystals into ultrasmall QDs. A disintegration mechanism induced by the high turbulent shear rate is suggested to account for their formation. The resulting small-size $MoSe_2$ QDs provide a high fraction of exposed atoms on edge sites, which significantly improves their electrocatalytic activity. Moreover, the TSM strategy was efficient in creating defects on the basal planes of $MoSe_2$ QDs, endowing additional active sites for electrocatalytic reactions. The presence of such a high fraction of edge sites and defects led us to apply these $MoSe_2$ QDs as an intriguing electrocatalyst for HER and regenerating redox couple in dye-sensitized solar cells (DSSCs).

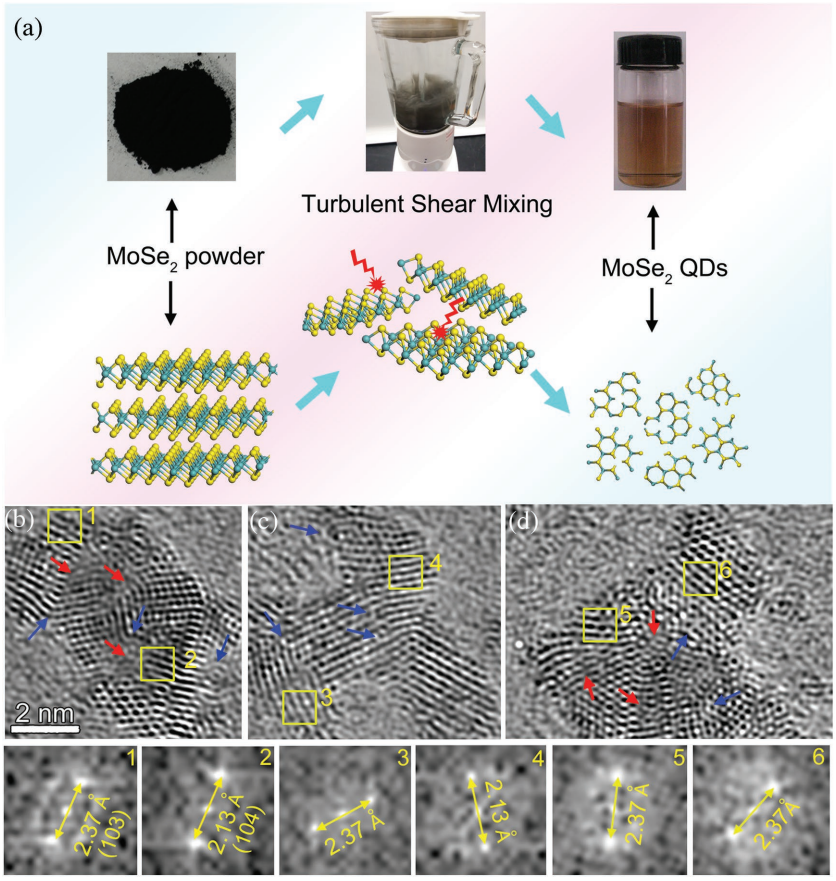

Figure 1. a) Schematic diagram of the TSM process for preparing $MoSe_2$ QDs from bulk $MoSe_2$. b–d) Stages of the disintegration process of $MoSe_2$ at the atomic scale. The HRTEM images are filtered in Fourier space using a mask to select the primary lattice frequencies and to remove the high-frequency noise above the information transfer limit. The lowest row shows fast Fourier transform patterns corresponding to the selected regions in (b–d), revealing the preferential (103) plane for disintegration of $MoSe_2$ into QDs.

The typical TSM process for preparing $MoSe_2$ QDs from bulk $MoSe_2$ is schematically illustrated in **Figure 1**a. A commercially available kitchen blender is adopted, which consists of six blades in various directions and is fitted with four baffles to suppress rotation of the liquid as a whole and to increase turbulence during the TSM process (Figure S1, Supporting Information). In a typical procedure, $MoSe_2$ powder, synthesized by the hydrothermal method, was added into the blender containing a mixture of 75 mL water and 75 mL isopropanol for TSM processing (Figure S2, Supporting Information). The selection of solvents used refers to the previous study by Ajayan and co-workers,[14] in order to keep the surface tension components of solvents well matched with that of $MoSe_2$ material (Table S1, Supporting Information), which is favorable for the preparation of $MoSe_2$ QDs by TSM technique and the stability of the targeted dispersion. After a predetermined-time of TSM processing, stable brown $MoSe_2$ QD (Figure 1a) dispersions can be obtained through centrifugation to remove concomitant $MoSe_2$ nanosheets.[2d]

To address the formation mechanism of $MoSe_2$ QDs by the TSM technique, fluid dynamics involving Reynolds number is invoked to analyze the underlying fluid interactions within a rotating blender.[2d] Reynolds number can be presented by the formula $Re_{Blade} = ND^2\rho/\eta$,[15] where N is the rotor speed, D is blade diameter, ρ and η are the liquid density and viscosity, respectively (see Table S2 in the Supporting Information for more details). When N is near maximum value, the Re_{Blade} can be calculated to be 2.72×10^5, which is far above the critical value $\approx 10^4$ where turbulence becomes fully developed.[16] Assuming that all of the input power is dissipated via turbulence, then the mean turbulence shear rate can be expressed as: $\dot{\gamma}_t = \sqrt{P/V\eta}$.[16] At a maximum N, P = 400 W and V = 0.15 L, we can obtain a $\dot{\gamma}_t$ of 1.24×10^4 s^{-1}. We believe such a high turbulent shear rate can not only successfully exfoliate LTD nanosheets,[2d,17] but also accounts for the formation of $MoSe_2$ QDs via further breaking up $MoSe_2$ crystal layers.[18] This disintegrating mechanism is corroborated by transmission electron microscopy (TEM) observation of the ex situ morphology evolution of products at different stages. As shown in Figure S3 (Supporting Information), bulk $MoSe_2$ was initially exfoliated into dispersive $MoSe_2$ nanosheets under the high turbulent shear

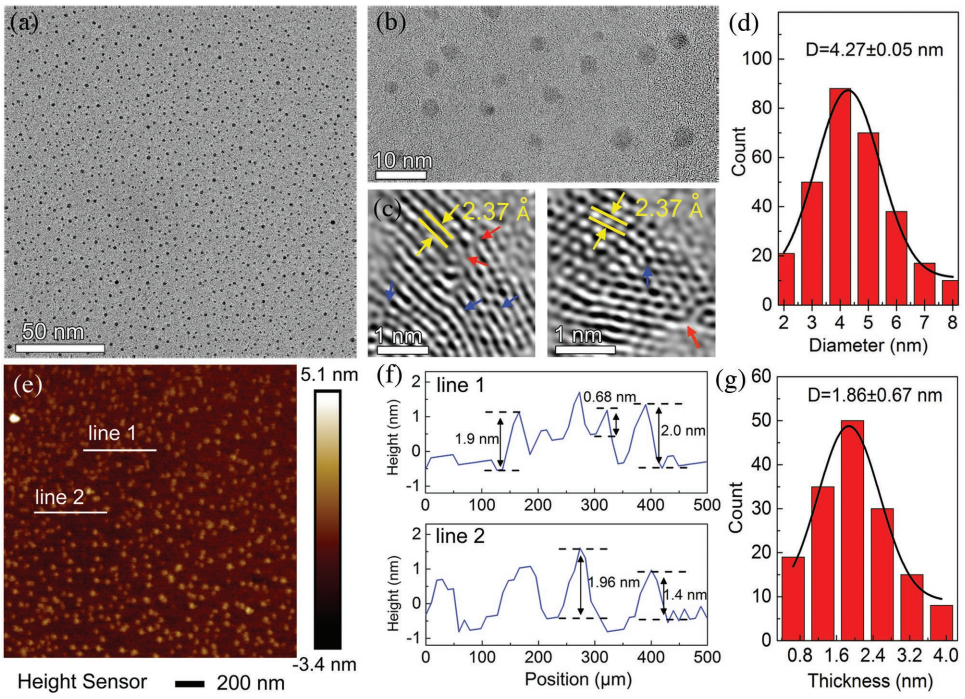

Figure 2. Morphology characterization of $MoSe_2$ QDs. a,b) Typical TEM bright-field images and c) HRTEM images of as-prepared $MoSe_2$ QDs. d) Statistical analysis of the size of $MoSe_2$ QDs measured by TEM. e) AFM image of $MoSe_2$ QDs. f) Height profiles along the white lines in (e). g) Statistical analysis of the heights of $MoSe_2$ QDs measured by AFM.

rate. Subsequently, the $MoSe_2$ nanosheets interspersed with $MoSe_2$ QDs gradually occurred. This observation of intermediate process provides a solid proof that the QDs originated from the initially exfoliated nanosheets. Further prolonging the TSM process, abundant $MoSe_2$ QDs with ultrasmall sizes are finally formed. In addition to $MoSe_2$ QDs, this disintegration mechanism also shows the universality in preparing QDs of other LTD materials (Figure S4, Supporting Information). High-resolution TEM (HRTEM) images (Figure 1b–d) of intermediate products are further acquired with disordered lattice fringes (marked by arrows), revealing $MoSe_2$ nanosheets could not maintain ideal 2D crystal structure under the high turbulent shear rate, instead were contorted to a highly defective structure,[6b] and then broken up into small QDs. By investigating the crystal structure of edges, we further found that $MoSe_2$ nanosheets preferentially disintegrate from (103) planes, which is also a preferred crystal plane during the growth of $MoSe_2$.

The structure of the as-obtained $MoSe_2$ QDs is characterized by TEM. **Figure 2**a evidences a large quantity of QDs with a mean size of 4.3 nm. HRTEM images show lattice fringes of these QDs are 2.37 Å, corresponding to the (103) plane of hexagonal $MoSe_2$. It is worth to note that discontinuous (red arrows) and contorted (blue arrows) lattice fringes are also clearly observed, indicating that the TSM technique can be used for preparing defect-laden QDs.[6b] This differs from the conventional ultrasonication method that generates QDs with high crystallization.[13b,19] Further morphology and thickness of $MoSe_2$ QDs were investigated by atomic force microscopy (AFM) measurement (Figure 2e–g). Height profiles reveal a thickness of 0.68–2 nm (Figure 2f), about 1–3 layers, since the thickness of single-layer $MoSe_2$ is about 0.65 nm (Figure S5, Supporting Information).[19a] This result is corroborated by statistical histogram in Figure 2g with a mean thickness of 1.86 nm. Compared to the bulk counterpart, the ultrasmall and defect-laden $MoSe_2$ QDs can provide a higher fraction of catalytic atoms on both basal planes and edges.

The surface chemical composition and valence states of $MoSe_2$ QDs was confirmed by the X-ray photoelectron spectroscopy (XPS). As shown in **Figure 3**a,b, the peaks around 228.9 and 232.2 eV correspond to Mo $3d_{5/2}$ and Mo $3d_{3/2}$, respectively, while the peaks at 54.5 and 55.3 eV can be attributed to Se $3d_{5/2}$ and Se $3d_{3/2}$ orbits, which are in good agreement with the binding energies of Mo^{4+} and Se^{2-} of $MoSe_2$.[7a] No signal from the Mo^{6+} was observed, indicating that there is no obvious oxidation of $MoSe_2$ QDs.[19] Figure 3c presents the Raman spectrum of $MoSe_2$ QDs. Two distinct Raman peaks at 238 and 285 cm^{-1} correspond to the out-of-plane (A_g^1) and in-plane (E_{2g}^1) Mo–Se vibrations of $MoSe_2$ QDs, respectively,[8] as illustrated in Figure S6 (Supporting Information). A_g^1 is typically preferentially excited for edge-terminated $MoSe_2$, while E_{2g}^1 is preferentially excited for terrace-terminated $MoSe_2$.[8] Compared with bulk $MoSe_2$, $MoSe_2$ QDs show a redshift by 5.4 cm^{-1} in E_{2g}^1 mode, analogous to that observed in boron nitride (BN) QDs due to small lateral dimensions.[20] Moreover, the E_{2g}^1 peak in the $MoSe_2$ QDs is also less pronounced (intensity is only 13% of A_g^1 peak) and broad. This means that the A_g^1 mode is preferentially excited in the as-prepared $MoSe_2$ QDs, confirming that the $MoSe_2$ QDs have more exposed catalytic edge sites.[8]

Further characterizations are performed by measuring the absorption spectrum and photoluminescence (PL)

ADVANCED SCIENCE NEWS
www.advancedsciencenews.com

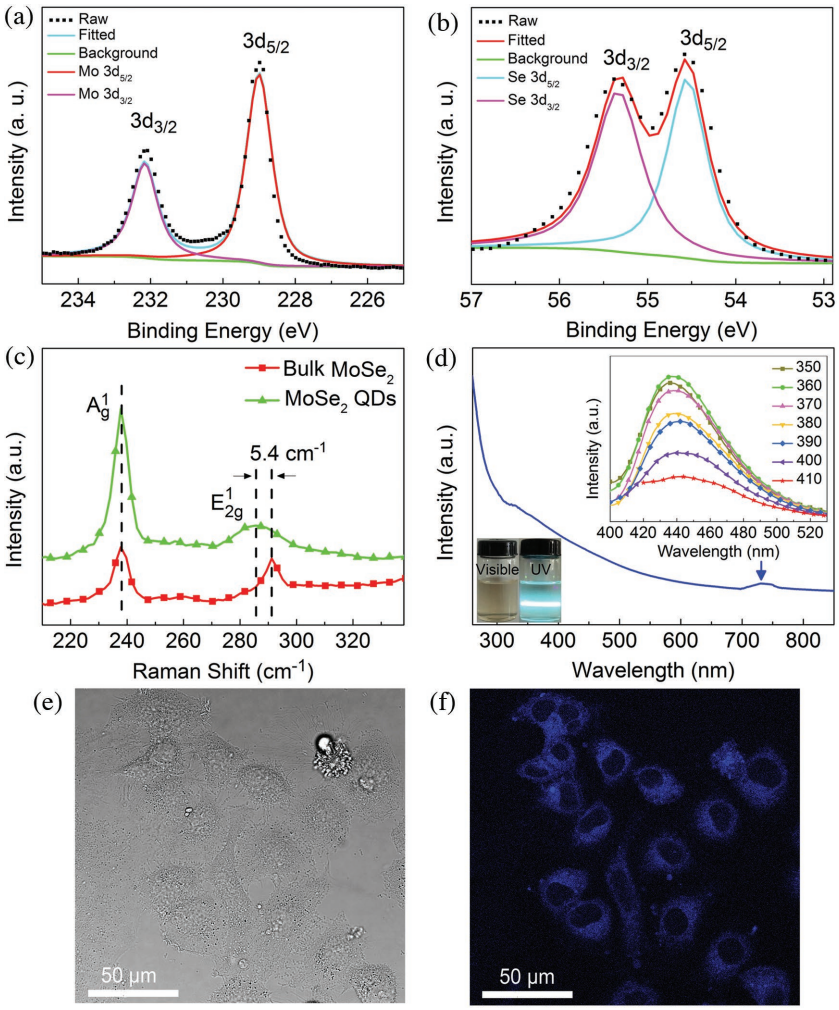

Figure 3. High-resolution XPS spectra of a) Mo 3d and b) Se 3d core levels. c) Raman spectrum of $MoSe_2$ QDs and bulk $MoSe_2$. d) UV–vis absorption spectrum of $MoSe_2$ QD dispersions. Inset: PL spectra of $MoSe_2$ QD dispersions under different excitation wavelengths, and optical photograph of $MoSe_2$ QD dispersions under visible and UV light. e) Bright-field image and f) corresponding confocal laser scanning microscopy image of HeLa living cells incubated with $MoSe_2$ QDs.

spectra of $MoSe_2$ QDs. Obviously, $MoSe_2$ QDs show a broad absorbance pattern in the visible region and near-infrared (NIR) band (Figure 3d). Strong fluorescence also can be seen from the optical photograph under 365 nm UV illumination (inset in Figure 3d). The small peak at 745 nm (≈1.66 eV) is generally ascribed to excitonic emission from $MoSe_2$, which is blueshifted compared with single-layer nanosheets (1.57 eV).[21] This is mainly attributed to a quantum size confinement effect, i.e., the optical absorption exhibiting a strong blueshift when the lateral dimensions of nanomaterials are reduced to below 50 nm.[22] Such effect is further evidenced in PL spectra (inset in Figure 3d) of $MoSe_2$ QDs, which show a characteristic emission peak at 445 nm under excitation of 360 nm wavelength. The emission is strongly blueshifted compared to that for single-layer $MoSe_2$ nanosheet.[21] With increasing the excitation wavelength, the emission peak shifts to the red and remain obvious intensity at 400 nm excitation wavelength. Such strong excitation-dependent features in PL reveal the polydispersity of $MoSe_2$ QDs,[22] which ensures the remarkable fluorescence of HeLa living cells when incubated with $MoSe_2$ QDs (Figure 3e,f). Generally, the polydispersity is owing to the difference in the particle size and the presence of surface trap states of defective $MoSe_2$ QDs.[22,23]

As typical applications, we have demonstrated the defect-laden $MoSe_2$ QDs as enhanced electrocatalysts toward the reduction of I_3^- in DSSCs and for HER as well. The catalytic activities toward the reduction of I_3^- are evaluated by cyclic voltammetry (CV) measurements in **Figure 4**a and Figure S7 (Supporting Information). Two pairs of typical oxidation and reduction peaks (Ox-1/Red-1, Ox-2/Red-2) can be well distinguished, corresponding to the reaction of Equations (1) and (2),[24] respectively. Since the catalysts in DSSCs are responsible for catalyzing reduction of I_3^- to I^-, the characteristics of the left pair (Ox-1/Red-1) are at the main concern of our analysis.

$$I_3^- + 2e^- \leftrightarrow 3I^- \quad (1)$$

$$3I_2 + 2e^- \leftrightarrow 2I_3^- \quad (2)$$

Generally, high current densities and low separation between Red-1 and Ox-1 peaks (E_{pp}) indicate excellent catalytic activity toward reduction of I_3^-.[25] From **Table 1**, $MoSe_2$ QD electrode has a higher cathodic current density and a smaller E_{pp} value of 0.32 V than bulk $MoSe_2$ and Pt electrodes, suggesting a faster catalytic rate for I^- regeneration on the surface of $MoSe_2$ QD electrode.[25] To further gain insight into the charge transfer process at the electrode–electrolyte interface, electrochemical impedance spectra measurements are also performed (Figure 4b and Table 1).[26] All three electrodes have nearly the same absolute series resistance (R_s), revealing a negligible role of R_s on differences in the electrocatalytic performance of different electrodes. However, the $MoSe_2$ QD electrode exhibits a lower charge transfer resistance (R_{ct}) of 5.46 Ω than 9.41 Ω of bulk $MoSe_2$ electrode, implying faster charge transport at the $MoSe_2$ QD electrode–electrolyte interface. Generally, faster charge transport means higher exchange current density, which is evidenced by the Tafel polarization curves (Figure S8, Supporting Information).

The excellent catalytic activities of $MoSe_2$ QDs make them promising candidates for replacing Pt catalyst, which has a low abundance on the earth and is of high cost.[24] Figure 4c compares the photovoltaic performance of DSSCs assembled with various counter electrodes (CEs). When bulk $MoSe_2$ is used as CE, the open-circuit voltage (V_{oc}), short-circuit current density (J_{sc}), fill factor (FF), and power conversion

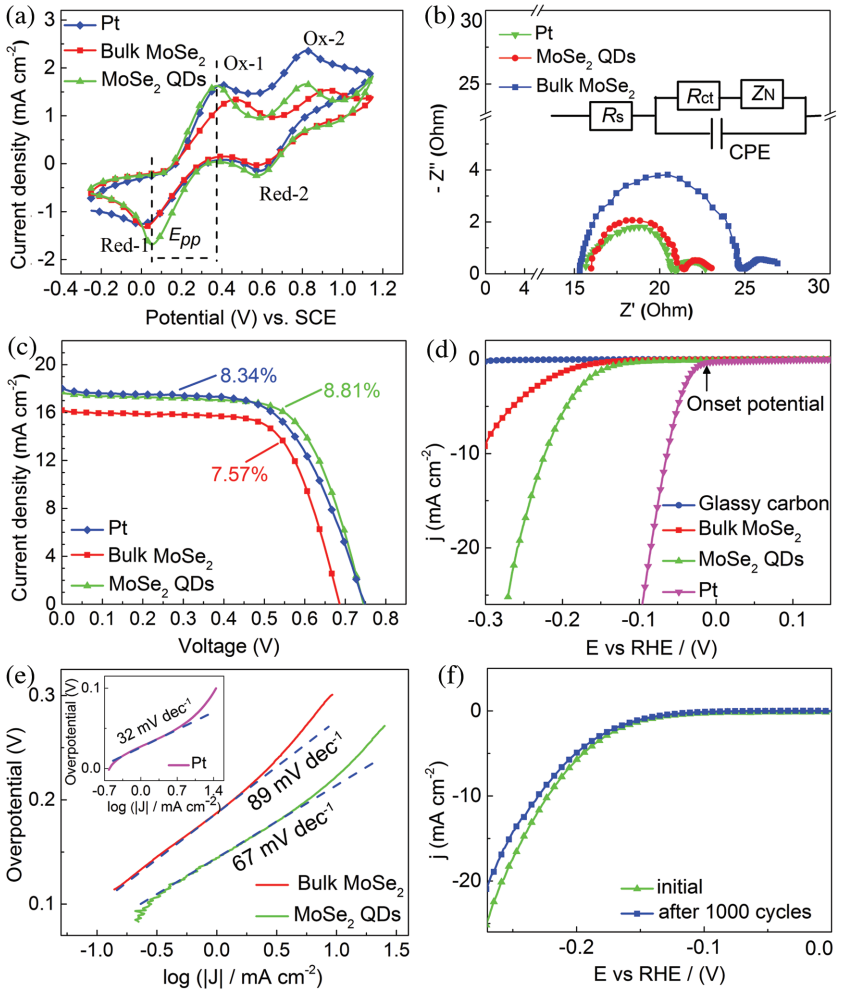

Figure 4. Electrocatalysis applications of $MoSe_2$ QDs in DSSCs (a–c) and HER (d–f). a) CV curves of Pt, $MoSe_2$ QDs, and bulk $MoSe_2$ CEs, obtained in acetonitrile solution containing 10.0×10^{-3} M LiI, 1.0×10^{-3} I_2, and 0.1 M $LiClO_4$ (scan rate: 50 mV s^{-1}). b) Electrochemical impedance spectra of above three CEs, obtained with two identical electrodes in the same electrolyte as that used in DSSCs. Inset shows the equivalent circuit used in DSSCs. c) Photocurrent density–voltage (*J*–*V*) curves of DSSCs constructed using above three electrodes. d) LSV polarization curves and e) the corresponding Tafel plots of commercial Pt, bulk $MoSe_2$, and $MoSe_2$ QDs, obtained in 0.5 M H_2SO_4 electrolyte at a scan rate of 2 mv s^{-1}. f) LSV polarization curves for $MoSe_2$ QD catalysts before and after 1000 times of CV cycles.

efficiency (PCE) are 0.70 V, 16.10 mA cm^{-2}, 0.68, and 7.57%, respectively (Table 1). This PCE value is apparently lower than 8.34% achieved from Pt CE. However, by replacing the bulk $MoSe_2$ CE with $MoSe_2$ QD CE, the PCE of the corresponding DSSC increases to 8.81%. Such impressive PCE not only can rival that of Pt CE, but also is outstanding among the LTD CEs (Table S3, Supporting Information).

For the application of HER, catalytic activities of $MoSe_2$ QDs as well as bulk $MoSe_2$ and Pt, are probed by linear sweep voltammetry (LSV) in 0.5 M H_2SO_4 using a three-electrode configuration. As shown in Figure 4d, the Pt catalyst exhibits extremely high HER catalytic activity with a near zero onset potential (i.e., the potential at which the HER reactivity begins,[27] as marked in Figure 4d) and large current density. Contrarily, bulk $MoSe_2$ shows very weak HER performance with a low cathodic current density and high onset potential. Significant H_2 evolution (J = 10 mA cm^{-2}) is not achieved until –300 mV versus reversible hydrogen electrode. However, by replacing the bulk $MoSe_2$ with $MoSe_2$ QDs, the onset of catalytic activity shifts to a much more positive potential –124 mV, beyond which the cathodic current increases rapidly under more negative potentials. In addition, significant H_2 evolution is also found at a lower voltage of –221 mV (J = 10 mA cm^{-2}), indicating superior electrocatalytic activity of $MoSe_2$ QDs than bulk $MoSe_2$. Figure 4e presents Tafel slopes of different electrodes, which is an intrinsic property of electrocatalysts and is typically determined by the rate-limiting step of the HER.[28] It can be determined by Tafel plots where their linear portions are fit to the Tafel equation ($\eta = b \times \log j + a$, in which j is the current density and b is the Tafel slope). From Figure 4e, Tafel slopes of Pt, bulk $MoSe_2$, and $MoSe_2$ QDs are 32, 89, and 67 mV dec^{-1}, respectively. The smaller Tafel slope of $MoSe_2$ QDs than bulk $MoSe_2$ is advantageous for practical applications since it will lead to a faster increment of HER rate with increasing overpotential.[11b] Besides the HER activity, the durability is another significant quality for an advanced electrocatalysts. Figure 4f shows the comparison polarization curves for the $MoSe_2$ QD catalysts before and after 1000 cycles. Slight activity loss is observed, which may be caused by the mild oxidation of $MoSe_2$ QDs into MoO_3 (Figure S9, Supporting Information), or the remaining H_2 bubbles on the surface of the electrode that hinder the HER.[29]

Table 2 compares the HER performance of various $MoSe_2$ nanostructures. Obviously, $MoSe_2$ QD shows excellent HER activity among the undoped $MoSe_2$ catalysts such as $MoSe_2$ nanosheets,[30] porous $MoSe_2$ nanosheets,[9] and

Table 1. Parameters of electrochemical and photovoltaic performance using different CEs.

CEs	V_{oc} [V]	J_{sc} [mA cm^{-2}]	FF [%]	PCE [%]	R_s [Ω]	R_{ct} [Ω]	E_{pp} [mV]
Pt	0.75	17.83	0.63	8.34	15.66	4.01	440
$MoSe_2$ QDs	0.74	17.56	0.67	8.81	15.96	5.46	320
Bulk $MoSe_2$	0.70	16.10	0.68	7.57	15.35	9.41	480

Table 2. Comparison of HER performance of various $MoSe_2$ nanostructures in 0.5 M H_2SO_4.

$MoSe_2$ nanostructures	Method	Onset potential[a)] [V]	Tafel slope [mV dec^{-1}]	Ref.
$MoSe_2$ QDs	TSM	−0.12	67	Our work
Porous $MoSe_2$ nanosheet	Liquid exfoliation	−0.07	80	[9]
$MoSe_2$ nanosheet	Colloidal synthesis	−0.17	98	[30]
$MoSe_2$ film	CVD	−0.2	105–120	[8]
S-doped $MoSe_2$ nanosheet	Reflux method	−0.09	60	[29]
$MoSe_2$ nanosheet/rGO	Hydrothermal	−0.05 to −0.125	67–69	[7a,10b]
$MoSe_2$ nanosheet/carbon fiber	Solvothermal	−0.07 to −0.145	69–76	[11a]
$MoSe_2$ film/carbon fiber	CVD	−0.11	59.8	[11b]
$MoSe_2$ nanosheet/carbon nanotube	Solvothermal	−0.07	58	[12]

[a)]Onset potential: the potential at which the HER reactivity begins.

$MoSe_2$ films.[8] Even, our $MoSe_2$ can rival the S-doped $MoSe_2$ nanosheets[29] or $MoSe_2$-based composites.[7a,10b,11,12] The excellent catalytic activity of defect-laden $MoSe_2$ QDs can be attributed to two advantageous peculiarities. First, compared with their bulk counterpart, the ultrasmall size of $MoSe_2$ QDs provides an enhanced edge to basal plane ratio, hence resulting in higher catalytic activities from reactive edges.[31] Second, a large amount of defect sites have been created on the basal planes of $MoSe_2$ QDs, which is also favorable for catalytic reactions.[6b,9] Finally, it is worth noting that the HER performance of $MoSe_2$ QDs can be further improved through optimizing electrode mass/area or by mixing in carbon material such as graphene to improve electrical properties of the catalyst.[32]

In summary, we have demonstrated a novel "turbulent shear mixing" method to successfully engineer the nanostructure of $MoSe_2$ catalysts with prolific catalytic edge and basal-plane sites. With this approach, ultrasmall $MoSe_2$ QDs with a mean lateral size of 4.3 nm can be prepared that provide a high fraction of atoms in edge sites, which significantly improves the catalytic activity of the QDs. Moreover, the TSM was also found to generate abundant defective sites in the $MoSe_2$ QDs via the violent disintegration process, producing additional catalytic active sites. Thanks to these unique properties, the defect-laden $MoSe_2$ QDs have shown excellent electrocatalysis in both HER and DSSCs. We believe the current study provides a new paradigm for engineering LTD materials with prolific active sites for enhanced electrocatalysis.

Supporting Information

Supporting Information is available from the Wiley Online Library or from the author.

Acknowledgements

C.Y.Z. and Y.H. contributed equally to this work. L.T.S. thanks Prof. Rodney S. Ruoff from the Center for Multidimensional Carbon Materials, Institute for Basic Science in Korea for polishing this paper carefully. This work was supported by the 973 Program (Grant No. 2015CB352106), the National Natural Science Foundation of China (Grant Nos. 61574034, 51372039, and 61674029), the Jiangsu Province Science and Technology Support Program (Grant Nos. BK20141118 and BK20151417), the Fundamental Research Funds for the Central Universities, and the Research Innovation Program for College Graduates of Jiangsu Province (KYLX16_0219).

Conflict of Interest

The authors declare no conflict of interest.

[1] a) K. S. Novoselov, A. K. Geim, S. V. Morozov, D. Jiang, Y. Zhang, S. V. Dubonos, I. V. Grigorieva, A. A. Firsov, *Science* **2004**, *306*, 666; b) Q. H. Wang, K. Kalantar-Zadeh, A. Kis, J. N. Coleman, M. S. Strano, *Nat. Nanotechnol.* **2012**, *7*, 699; c) F. N. Xia, H. Wang, Y. C. Jia, *Nat. Commun.* **2014**, *5*, 4458.

[2] a) K. F. Mak, C. Lee, J. Hone, J. Shan, T. F. Heinz, *Phys. Rev. Lett.* **2010**, *105*, 136805; b) V. Nicolosi, M. Chhowalla, M. G. Kanatzidis, M. S. Strano, J. N. Coleman, *Science* **2013**, *340*, 1226419; c) Y. Huang, J. Wu, X. Xu, Y. D. Ho, G. X. Ni, Q. Zou, G. K. W. Koon, W. J. Zhao, A. H. C. Neto, G. Eda, C. M. Shen, B. Özyilmaz, *Nano Res.* **2013**, *6*, 200; d) K. R. Paton, E. Varrla, C. Backes, R. J. Smith, U. Khan, A. O'Neill, C. Boland, M. Lotya, O. M. Istrate, P. King, T. Higgins, S. Barwich, P. May, P. Puczkarski, I. Ahmed, M. Moebius, H. Pettersson, E. Long, J. Coelho, S. E. O'Brien, E. K. McGuire, B. M. Sanchez, G. S. Duesberg, N. McEvoy, T. J. Pennycook, C. Downing, A. Crossley, V. Nicolosi, J. N. Coleman, *Nat. Mater.* **2014**, *13*, 624.

[3] a) J. Z. Chen, X. J. Wu, L. S. Yin, B. Li, X. Hong, Z. X. Fan, B. Chen, C. Xue, H. Zhang, *Angew. Chem. Int. Ed.* **2015**, *54*, 1210; b) Y. F. Yu, S. Y. Huang, Y. P. Li, S. N. Steinmann, W. T. Yang, L. Y. Cao, *Nano Lett.* **2014**, *14*, 553; c) J. Zhang, S. Najmaei, H. Lin, J. Lou, *Nanoscale* **2014**, *6*, 5279; d) X. Y. Gong, Y. Q. Gu, N. Li, H. Y. Zhao, C. J. Jia, Y. P. Du, *Inorg. Chem.* **2016**, *55*, 3992.

[4] a) B. O'Regan, M. Grätzel, *Nature* **1991**, *353*, 737; b) D. V. Esposito, S. T. Hunt, A. L. Stottlemyer, K. D. Dobson, B. E. McCandless, R. W. Birkmire, J. G. Chen, *Angew. Chem. Int. Ed.* **2010**, *49*, 9859.

[5] a) Y. F. Sun, S. Gao, F. C. Lei, Y. Xie, *Chem. Soc. Rev.* **2015**, *44*, 623; b) B. Hinnemann, P. G. Moses, J. Bonde, K. P. Jørgensen, J. H. Nielsen, S. Horch, I. Chorkendorff, J. K. Nørskov, *J. Am. Chem. Soc.* **2005**, *127*, 5308.

[6] a) T. F. Jaramillo, K. P. Jørgensen, J. Bonde, J. H. Nielsen, S. Horch, I. Chorkendorff, *Science* **2007**, *317*, 100; b) J. F. Xie, H. Zhang, S. Li, R. X. Wang, X. Sun, M. Zhou, J. F. Zhou, X. W. Lou, Y. Xie, *Adv. Mater.* **2013**, *25*, 5807; c) Z. Q. Liu, H. Y. Zhao, N. Li, Y. Zhang, X. Y. Zhang, Y. P. Du, *Inorg. Chem. Front.* **2016**, *3*, 313.
[7] a) H. Tang, K. P. Dou, C. C. Kaun, Q. Kuang, S. H. Yang, *J. Mater. Chem. A* **2014**, *2*, 360; b) Z. Gholamvand, D. McAteer, C. Backes, N. McEvoy, A. Harvey, N. C. Berner, D. Hanlon, C. Bradley, I. Godwin, A. Rovetta, M. E. G. Lyons, G. S. Duesberga, J. N. Coleman, *Nanoscale* **2016**, *8*, 5737.
[8] H. T. Wang, D. S. Kong, P. Johanes, J. J. Cha, G. Y. Zheng, K. Yan, N. Liu, Y. Cui, *Nano Lett.* **2013**, *13*, 3426.
[9] Z. Y. Lei, S. J. Xu, P. Y. Wu, *Phys. Chem. Chem. Phys.* **2016**, *18*, 70.
[10] a) S. J. Xu, Z. Y. Lei, P. Y. Wu, *J. Mater. Chem. A* **2015**, *3*, 16337; b) Z. Q. Liu, N. Li, H. Y. Zhao, Y. P. Du, *J. Mater. Chem. A* **2015**, *3*, 19706.
[11] a) B. Qu, X. B. Yu, Y. J. Chen, C. L. Zhu, C. Y. Li, Z. X. Yin, X. T. Zhang, *ACS Appl. Mater. Interfaces* **2015**, *7*, 14170; b) D. S. Kong, H. T. Wang, J. J. Cha, M. Pasta, K. J. Koski, J. Yao, Y. Cui, *Nano Lett.* **2013**, *13*, 1341.
[12] Y. P. Huang, H. Y. Lu, H. H. Gu, J. Fu, S. Y. Mo, C. Wei, Y. E. Miao, T. X. Liu, *Nanoscale* **2015**, *7*, 18595.
[13] a) D. Gopalakrishnan, D. Damien, B. Li, H. Gullappalli, V. K. Pillai, P. M. Ajayanb, M. M. Shaijumon, *Chem. Commun.* **2015**, *51*, 6293; b) S. J. Xu, D. Li, P. Y. Wu, *Adv. Funct. Mater.* **2015**, *25*, 1127.
[14] J. F. Shen, Y. M. He, J. J. Wu, C. T. Gao, K. Keyshar, X. Zhang, Y. C. Yang, M. X. Ye, R. Vajtai, J. Lou, P. M. Ajayan, *Nano Lett.* **2015**, *15*, 5449.
[15] A. T. Utomo, M. Baker, A. W. Pacek, *Chem. Eng. Res. Des.* **2008**, *86*, 1397.
[16] a) J. A. Boxall, C. A. Koh, E. D. Sloan, A. K. Sum, D. T. Wu, *Langmuir* **2012**, *28*, 104; (b) R. Wengeler, H. Nirschl, *J. Colloid Interface Sci.* **2007**, *306*, 262.
[17] a) E. Varrla, C. Backes, K. R. Paton, A. Harvey, Z. Gholamvand, J. McCauley, J. N. Coleman, *Chem. Mater.* **2015**, *27*, 1129; b) E. Varrla, K. R. Paton, C. Backes, A. Harvey, R. J. Smith, J. McCauley, J. N. Coleman, *Nanoscale* **2014**, *6*, 11810.
[18] C. Y. Zhu, F. Xu, L. Zhang, M. L. Li, J. Chen, S. H. Xu, G. G. Huang, W. H. Chen, L. T. Sun, *Chem. - Eur. J.* **2016**, *22*, 7357.
[19] a) X. Zhang, Z. C. Lai, Z. D. Liu, C. L. Tan, Y. Huang, B. Li, M. T. Zhao, L. H. Xie, W. Huang, H. Zhang, *Angew. Chem. Int. Ed.* **2015**, *54*, 5425; b) L. H. Yuwen, J. J. Zhou, Y. Q. Zhang, Q. Zhang, J. Y. Shan, Z. M. Luo, L. X. Weng, Z. G. Teng, L. H. Wang, *Nanoscale* **2016**, *8*, 2720.
[20] L. X. Lin, Y. X. Xu, S. W. Zhang, I. M. Ross, A. C. M. Ong, D. A. Allwood, *Small* **2014**, *10*, 60.
[21] P. Tonndorf, R. Schmidt, P. Böttger, X. Zhang, J. Börner, A. Liebig, M. Albrecht, C. Kloc, O. Gordan, D. R. T. Zahn, S. M. D. Vasconcellos, R. Bratschitsch, *Opt. Express* **2013**, *21*, 4908.
[22] a) D. Gopalakrishnan, D. Damien, M. M. Shaijumon, *ACS Nano* **2014**, *8*, 5297; b) X. P. Ren, L. Q. Pang, Y. X. Zhang, X. D. Ren, H. B. Fanac, S. Z. Liu, *J. Mater. Chem. A* **2015**, *3*, 10693; c) J. P. Wilcoxon, G. A. Samara, *Phys. Rev. B* **1995**, *51*, 7299.
[23] a) V. Stengl, J. Henych, *Nanoscale* **2013**, *5*, 3387; b) D. B. Shinde, V. K. Pillai, *Chem. - Eur. J.* **2012**, *18*, 12522.
[24] F. Gong, H. Wang, X. Xu, G. Zhou, Z. S. Wang, *J. Am. Chem. Soc.* **2012**, *134*, 10953.
[25] J. H. Guo, Y. T. Shi, Y. T. Chua, T. L. Ma, *Chem. Commun.* **2013**, *49*, 10157.
[26] X. X. Chen, Q. W. Tang, B. L. He, L. Lin, L. M. Yu, *Angew. Chem. Int. Ed.* **2014**, *53*, 10799.
[27] A. B. Laursen, S. Kegnæs, S. Dahl, I. Chorkendorff, *Energy Environ. Sci.* **2012**, *5*, 5577.
[28] a) N. Pentland, J. O. M. Bockris, E. Sheldon, *J. Electrochem. Soc.* **1957**, *104*, 182; b) B. E. Conway, B. V. Tilak, *Electrochim. Acta* **2002**, *47*, 3571.
[29] C. Xu, S. J. Peng, C. L. Tan, H. X. Ang, H. T. Tan, H. Zhang, Q. Y. Yan, *J. Mater. Chem. A* **2014**, *2*, 5597.
[30] X. L. Zhou, J. Jiang, T. Ding, J. J. Zhang, B. C. Pan, J. Zuo, Q. Yang, *Nanoscale* **2014**, *6*, 11046.
[31] Z. Gholamvand, D. McAteer, A. Harvey, C. Backes, J. N. Coleman, *Chem. Mater.* **2016**, *28*, 2641.
[32] D. McAteer, Z. Gholamvand, N. McEvoy, A. Harvey, E. O. Malley, G. S. Duesberg, J. N. Coleman, *ACS Nano* **2016**, *10*, 672.

Received: February 19, 2017
Revised: April 2, 2017
Published online: May 24, 2017

